PROCEEDINGS OF SPIE

SPIEDigitalLibrary.org/conference-proceedings-of-spie

Acute branch retinal artery occlusion segmentation based on Bayes posterior probability and deep learning

Guo, Chao, Zhu, Weifang, Wang, Meng, Liu, Ming, Chen, Zhongyue, et al.

Chao Guo, Weifang Zhu, Meng Wang, Ming Liu, Zhongyue Chen, Xinjian Chen, "Acute branch retinal artery occlusion segmentation based on Bayes posterior probability and deep learning," Proc. SPIE 12032, Medical Imaging 2022: Image Processing, 120323V (4 April 2022); doi: 10.1117/12.2611500

SPIE.

Event: SPIE Medical Imaging, 2022, San Diego, California, United States

Downloaded From: https://www.spiedigitallibrary.org/conference-proceedings-of-spie on 05 Apr 2022 Terms of Use: https://www.spiedigitallibrary.org/terms-of-use

Acute Branch Retinal Artery Occlusion Segmentation Based on Bayes Posterior Probability and Deep Learning

Chao Guo[1], Weifang Zhu[1], Meng Wang[1], Ming Liu[1], Zhongyue Chen[1], Xinjian Chen[1,2,*]
[1]School of Electronics and Information Engineering, Soochow University, Suzhou, Jiangsu Province 215006, China
[2]State Key Laboratory of Radiation Medicine and Protection, Soochow University, Suzhou, Jiangsu Province, 215123, China

ABSTRACT

Branch retinal artery occlusion (BRAO) is an ophthalmic emergency. Acute BRAO is a clinical manifestation of BRAO. Due to its various shapes, locations and the blurred boundary, the automatic segmentation of acute BRAO is very challenging. To tackle these problems, we propose a novel method based on deep learning for automatic acute BRAO segmentation in optical coherence tomography (OCT) image. In this method, a novel Bayes posterior attention network, named as BPANet, is proposed for precise segmentation of the lesion. Our major contributions include: (1) A novel Bayes posterior probability based spatial attention module is used to enhance the information of lesion region. (2) An effective max-pooling and average-pooling channel attention module is embedded into BPANet to improve the effectiveness of the feature extraction. The proposed method is evaluated on 472 OCT B-scan images with a 4-fold cross validation strategy. The mean and standard deviation of Dice similarity coefficient, true positive rate, accuracy and intersection over union are 85.48±1.75%, 88.84±1.19%, 98.63±0.48% and 76.88±2.92%, respectively. The primary results show the effectiveness of the proposed method.

Keywords: Optical coherence tomography, acute branch retinal artery occlusion, Bayes posterior probability, channel attention

1. INTRODUCTION

Branch retinal artery occlusion (BRAO) is a potentially devastating visual disorder usually caused by closure of the vessel, which could lead to blindness [1]. Acute BRAO is a clinical manifestation of BRAO, which is characterized histopathologically by inner retinal edema [2]. The effective treatment for patients needs quantitative analysis of the lesion region. Therefore, the segmentation of acute BRAO has import clinical relevance.

Recently, optical coherence tomography (OCT) is widely used in the auxiliary diagnosis and treatment of various retinal diseases, which could provide in vivo, cross-sectional image of retina [3]. Figure 1 is a 2D OCT B-scan image with acute BRAO, in which acute BRAO occurs in the inner retinal region with high intensity value. At present, most studies on BRAO are focused on its clinical analysis [4,5]. There are very few studies focused on its automatic segmentation and analysis. Our previous work proposed a Bayes posterior probability, graph search and graph cut based framework for automatic segmentation of BRAO [6].

In this paper, an automatic segmentation method for acute BRAO based on Bayes posterior probability and deep learning is proposed, which includes initial segmentation and precise segmentation. In the initial segmentation stage, the inner retinal region is extracted as the region of interest (ROI) by using dynamic planning algorithm. In the precise segmentation stage, a novel Bayes posterior attention network (named as BPANet) is proposed. A novel spatial attention mechanism named as Bayes spatial attention (BSA) module is proposed and embedded into the forefront of the BPANet to enhance and locate the lesion region in pixel-wise using Bayes posterior probability, which can help the network know where to look. Inspired by convolutional block attention module (CBAM) [7] and efficient channel attention (ECA) module [8], a novel channel attention module— max-pooling and average-pooling channel attention (MACA) module is proposed to improve the performance of encoder, making the network know what to look.

* Corresponding author: E-mail: xjchen@suda.edu.cn.

Medical Imaging 2022: Image Processing, edited by Olivier Colliot, Ivana Išgum, Proc. of SPIE Vol. 12032, 120323V · © 2022 SPIE
1605-7422 · doi: 10.1117/12.2611500

Downloaded From: https://www.spiedigitallibrary.org/conference-proceedings-of-spie on 05 Apr 2022
Terms of Use: https://www.spiedigitallibrary.org/terms-of-use

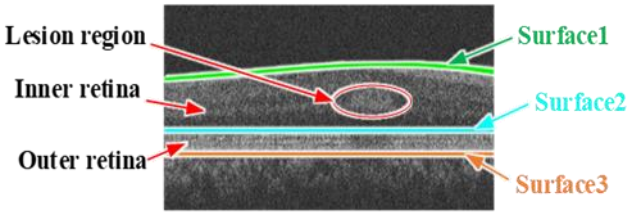

Figure 1. Original OCT B-scan and acute BRAO.

2. METHODS

The overall structure of the proposed automatic acute BRAO segmentation method is shown in Figure 2, which mainly contains two parts: initial segmentation and precise segmentation. First, the dynamic planning algorithm is adopted to extract the inner retina region as the ROI in the initial segmentation stage. Then the novel proposed BPANet is adopted for the precise segmentation, which mainly consists of BSA module, encoder with MACA module and decoder.

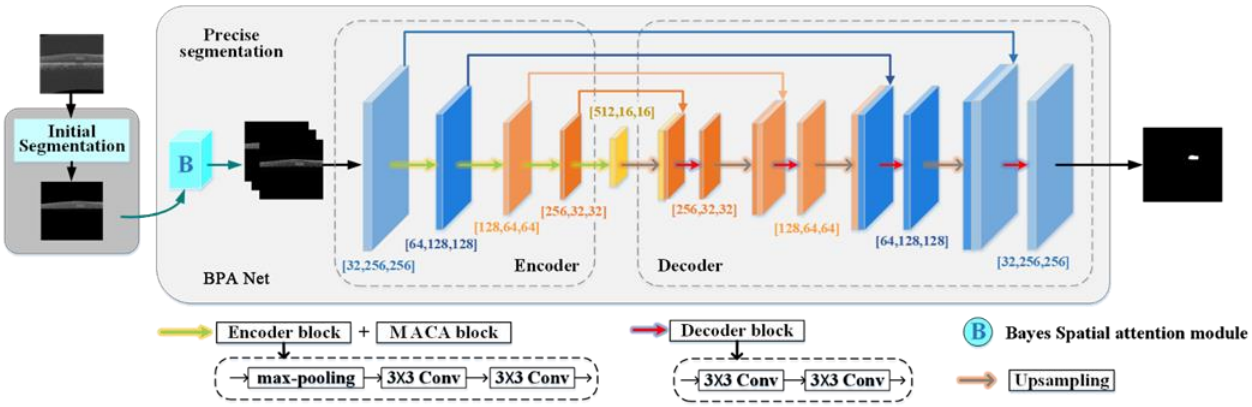

Figure 2. Flowchart of the proposed segmentation network. In initial segmentation, the inner retina region is extracted as the ROI. The precise segmentation network consists of three modules: BSA module, encoder with MACA module and decoder.

2.1 Initial segmentation

As shown in Figure 1, acute BRAO occurs in the inner retinal layers between Surface 1 and Surface 2. However, the overall intensity level of the outer retina region (between Surface 2 and Surface 3) is higher than that of the inner one, which is similar to the intensity of acute BRAO. In order to reduce the influence of outer retina region on acute BRAO segmentation, we extracted the inner retinal layer as ROI by referring to [9]. The cost function C, shown as Eq. (1), based on edge gradient is adopted and applied in the dynamic planning algorithm to find the Surface 1 and Surface 2.

$$C = \sum_{j=1}^{N} E_d + \lambda \sum_{j=2}^{N-1} (n_{j-1} + n_{j+1} - 2n_j)^2 \tag{1}$$

where n is the selected path of the j' th column, N is the columns of the image graph, E_d is an edge-based cost, and λ is a regularization constant which determines the smoothness of the path.

2.2 Precise segmentation-- Bayes posterior attention network

To precisely segment acute BRAO, inspired by U-Net [10], we propose a novel Bayes posterior attention network (BPANet). As shown in Figure2, the proposed BPANet mainly contains three components: BSA module, encoder with MACA module and decoder. The extracted ROI from initial segmentation is fed to the BSA module to construct the input of the precise segmentation network. Four encoder layers are used to form the encoder of the network.

Each encoder layer includes two 3×3 convolutions and a 2×2 max pooling operation with stride 2 for down sampling. Each convolutional kernel is followed by a rectified linear unit (ReLU). Besides, a MACA module is added behind each encoder layer to adjust the output feature map.

Downloaded From: https://www.spiedigitallibrary.org/conference-proceedings-of-spie on 05 Apr 2022
Terms of Use: https://www.spiedigitallibrary.org/terms-of-use

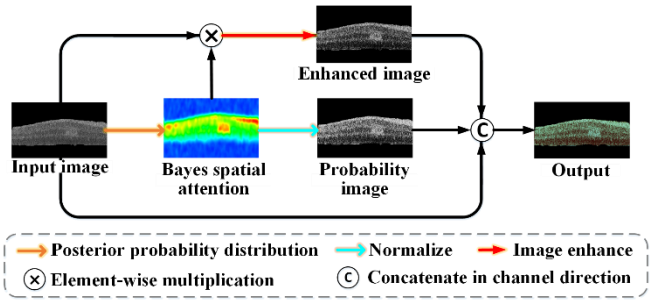

Figure 3. Diagram of BSA module. Bayes posterior probability is used to generate spatial attention to enhance the lesion region in this module.

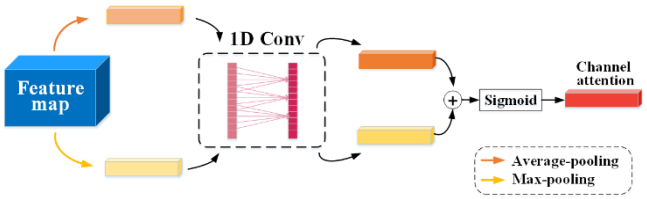

Figure 4. Diagram of MACA module. Average-pooling and max-pooling combine with a 1D convolution to generate channel attention map in this module.

2.3 Bayes spatial attention module

Inspired by spatial attention in CBAM [7], we design a Bayes spatial attention module based on Bayes posterior probability, which can enhance the lesion region in the ROI, as shown in Figure 3.

According to the intensity value I_p, we use Eq. (2) – (6) to calculate the posterior probability of being the object region for each pixel x_i. Thus, we can get the probability distribution of pixels.

$$P(x_i \in R_o \,|\, I_p) = \frac{P(I_p \,|\, R_o) \cdot P(R_o)}{P(I_p \,|\, R_o) \cdot P(R_o) + P(I_p \,|\, R_n) \cdot P(R_n)} \tag{2}$$

$$P(R_o) = \frac{hist(l_i \in l_o, x_i \in S)}{hist(x_i \in S)} \tag{3}$$

$$P(R_n) = \frac{hist(l_i \in l_n, x_i \in S)}{hist(x_i \in S)} \tag{4}$$

$$P(I_p \,|\, R_o) = \frac{hist(l_i \in l_o, x_i \in S)}{hist(x_i \in R_o)} \tag{5}$$

$$P(I_p \,|\, R_n) = \frac{hist(l_i \in l_n, x_i \in S)}{hist(x_i \in R_n)} \tag{6}$$

where S is the set of all the pixels x_i. x_i is marked as either disease I_o or normal I_n. R_o represents the disease region, and R_n represents the normal region. $P(R_o)$, $P(R_n)$, $P(I_p \,|\, R_o)$, $P(I_p \,|\, R_n)$, are calculated based on the data from the training set respectively.

Given an OCT B-scan F as input of BSA module. Firstly, the Bayes spatial attention map A_{BS} of F is generated by Eq. (2). The element $p_{x,y}$ of A_{BS} is calculated according to the intensity value $I_{x,y}$ in F. Second, the value of elements in

Downloaded From: https://www.spiedigitallibrary.org/conference-proceedings-of-spie on 05 Apr 2022
Terms of Use: https://www.spiedigitallibrary.org/terms-of-use

A_{BS} is normalized by multiplying 255 to [0, 255] to obtain the Bayes posterior probability attention graph F_B. Third, F and A_{BS} are multiplied at the elemental level and the result image is enhanced by adaptive histogram equalization [11] to obtain the enhanced image F_E. Finally, F, F_E and F_B are concatenated in the channel direction. In the test stage, the Bayes posterior probability is calculated according to the data of the training set.

The BSA module concatenates the information of the Bayesian posterior probability and the original image, and then fuses the information through convolution, helping the network attend to the lesion and learn the lesion feature.

2.4 Max-pooling and average-pooling channel attention

Figure 4 shows the details of max-pooling and average-pooling channel attention (MACA) module. In most channel attention, global average-pooling is widely used to aggregate global spatial information. Woo et al. [7] demonstrated that the combination of global average-pooling and max-pooling can improve the performance of channel attention. Therefore, we adopt average-pooling and max-pooling operations to generate two different spatial context descriptors. Inspired by ECA module [8], 1D convolution is adopted to properly conduct the interaction between adjacent channels and generate the channel weights without reducing the dimension. In addition, two different spatial context descriptors share the weights of 1D convolution. The output 1D channel attention map $A_c \in \mathbb{R}^{C\times1\times1}$ of the MACA module can be calculated as:

$$A_c = \sigma(C1D(AvgPool(F)) + C1D(MaxPool(F))) \tag{7}$$

where σ denotes the sigmoid function, *C1D* indicates 1D convolution.

Denote $F \in \mathbb{R}^{C\times H\times W}$ as the output feature map of an encoder layer. Finally, the input feature map F' of the next encoder layer can be represented as:

$$F' = A_C \otimes F \tag{8}$$

where $\otimes$ denotes element-wise multiplication.

3. RESULTS

3.1 Data description and implementation details

The proposed method performs four-fold cross validation on 472 2D retinal OCT B-scan images with acute BRAO. Each image has a size of 512×480. The retinal data is provided by the Joint Shantou International Eye Center. This study is approved by the Intuitional review board of Joint Shantou International Eye Center and adhered to the tenets of the Declaration of Helsinki. An experienced ophthalmologist was invited to manually label the disease areas as the ground truth.

The proposed method is implemented on the publicly available Pytorch platform and OpenCV libraries. The loss for segmentation model is minimized by the Adam optimizer with an initial learning rate of 1e-3. The segmentation network is trained on Nvidia GTX1080. In the training process, the training images are resized to 256×256 and the batch size is set to 16. Besides, in order to prevent overfitting, random rotation and scaling are adopted to carry out online data augmentation.

3.2 Evaluation metrics

To comprehensively demonstrate the effectiveness of the proposed method, Dice coefficient (Dice), true positive rate (TPR), intersection over union (IoU) and accuracy (ACC) are employed to quantitatively analyze the experimental results. We use Eq. (9) – (12) to calculate Dice [12], IoU [13], TPR [6] and ACC [6] respectively.

Downloaded From: https://www.spiedigitallibrary.org/conference-proceedings-of-spie on 05 Apr 2022
Terms of Use: https://www.spiedigitallibrary.org/terms-of-use

$$Dice = \frac{2 \cdot \sum_i^N p_i g_i}{\sum_i^N p_i^2 + \sum_i^N g_i^2} \tag{9}$$

$$IoU = \frac{|P \cap G|}{|P \cup G|} \tag{10}$$

$$TPR = \frac{TP}{TP + FN} \tag{11}$$

$$ACC = \frac{TP + TN}{TP + FP + TN + FN} \tag{12}$$

where P and G are the predicted binary segmentation mask and ground truth binary mask separately, $p_i \in P, g_i \in G$, and N is image size. *TP*, *FP*, *TN*, *FN* represent true positive, false positive, true negative and false negative respectively.

3.3 Results

The initial segmented ROIs are adopted to conduct experiments on different networks and attention modules. the original U-Net [10] is adopted as the baseline to prove the effectiveness of the proposed BSA module and MACA module. The ablation experiments and comparison experiments are conducted, the quantitative indicators and segmentation results are shown in Table 1 and Figure5, respectively. In addition, we also perform experiments to compare the segmentation performance with other excellent segmentation methods, including Attention U-Net [14], Seg-Net [15] and CE-Net [16].

As shown in Figure5, compared to the original U-Net, the proposed BPANet achieves better performance on small lesion segmentation as it can reduce the interference of normal regions with high intensity level such as retinal nerve fiber layer. As can be seen from Table 1, compared with other segmentation algorithms and modules [8,10,14,15,16,17], the proposed method has achieved best performance. Furthermore, the ablation experiment results listed in Table 1 indicates the effectiveness of the proposed BSA and MACA modules.

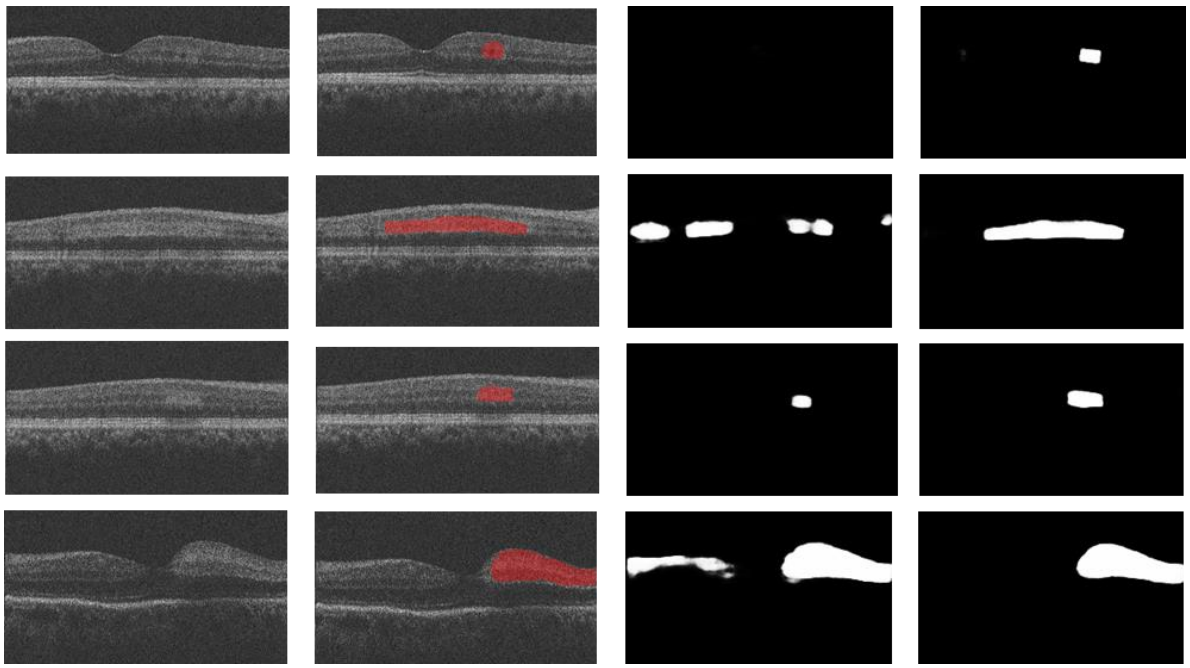

(a) (b) (c) (d)

Figure 5. Results of acute BRAO segmentation. (a) Original images; (b) ground truth (red regions); (c) results of U-net; (d) results of the proposed method.

Downloaded From: https://www.spiedigitallibrary.org/conference-proceedings-of-spie on 05 Apr 2022
Terms of Use: https://www.spiedigitallibrary.org/terms-of-use

Table 1. Segmentation results of different methods.

Method	Dice (%)	TPR (%)	IoU (%)	ACC (%)
Seg-Net	80.00±4.18	84.62±4.44	70.01±5.61	98.14±0.65
Attention U-Net	82.67±2.52	88.68±0.68	73.90±4.19	98.42±0.64
CE-Net	82.89±2.79	87.96±2.94	74.40±2.64	98.52±0.49
U-Net (baseline)	81.74±3.53	85.68±3.48	72.78±4.78	98.34±0.53
BSA + U-Net	83.11±2.38	86.15±2.25	74.19±3.54	98.53±0.42
U-Net + MACA	83.29±2.50	87.00±1.49	74.38±3.43	98.47±0.46
BSA + U-Net + SE [17]	84.93±1.94	87.78±2.11	76.14±3.24	98.60±0.45
BSA + U-Net + ECA	84.46±2.02	87.11±1.67	75.86±3.16	98.62±0.45
Our method	**85.48±1.75**	**88.84±1.19**	**76.88±2.92**	**98.63±0.48**

4. CONCLUSIONS

In this paper, we propose a novel Bayes posterior probability and deep learning-based method to accurately segment the acute BRAO in OCT images. The proposed method mainly consists of two stages: the inner retina region extraction based on dynamic planning algorithm and the precise segmentation by the proposed BPANet. The proposed method was evaluated on 472 OCT B-scans with a 4-fold cross validation strategy. The results show that, compared with other excellent algorithms, the proposed method has improved the segmentation performance significantly.

5. ACKNOWLEDGEMENTS

This work was supported in part by the National Key Research and Development Program of China under Grant 2018YFA0701700, in part by the National Nature Science Foundation of China under Grant U20A20170.

REFERENCES

[1] Parcero, Cíntia Maria Felix Medrado, et al., "Optical coherence tomography findings in acute phase of branch retinal artery occlusion: case report," Arquivos brasileiros de oftalmologia 73(2), 189-192 (2010).
[2] Goldenberg-Cohen, Nitza, et al., "Molecular and Histological Changes Following Central Retinal Artery Occlusion in a Mouse Model," Experimental Eye Research 87(4), 327–333 (2008).
[3] Abràmoff, M. D., et al., "Retinal Imaging and Image Analysis," IEEE Reviews in Biomedical Engineering 3(3), 169–208 (2010).
[4] Leung, C. K. S., et al., "In Vivo Measurements of Macular and Nerve Fibre Layer Thickness in Retinal Arterial Occlusion," Eye 21(12), 1464–1468 (2007).
[5] Asefzadeh, Baharak, and Kimberly Ninyo, "Longitudinal analysis of retinal changes after branch retinal artery occlusion using optical coherence tomography," Optometry-Journal of the American Optometric Association, 79(2), 85-89 (2008).
[6] Guo, Jingyun, et al., "A framework for classification and segmentation of branch retinal artery occlusion in SD-OCT," IEEE Transactions on Image Processing 26(7), 3518-3527 (2017).
[7] Woo, Sanghyun, et al., "Cbam: Convolutional block attention module," in Proceedings of the European conference on computer vision (ECCV), 3-19 (2018).
[8] Wang, Qilong, et al., "ECA-net: Efficient channel attention for deep convolutional neural networks," in Proceedings of the IEEE/CVF Conference on Computer Vision and Pattern Recognition, 11534-11542 (2020).
[9] Thomas, Martini, Jørgensen, et al., "Enhancing the signal-to-noise ratio in ophthalmic optical coherence tomography by image registration—method and clinical examples," Journal of Biomedical Optics, 12(4), 1-10 (2006).
[10] Ronneberger, Olaf, et al., "U-net: Convolutional networks for biomedical image segmentation," in International Conference on Medical image computing and computer-assisted intervention, 234-241 (2015).

Downloaded From: https://www.spiedigitallibrary.org/conference-proceedings-of-spie on 05 Apr 2022
Terms of Use: https://www.spiedigitallibrary.org/terms-of-use

[11] Stark, J. Alex, "Adaptive image contrast enhancement using generalizations of histogram equalization," IEEE Transactions on image processing, 9(5), 889-896 (2000).
[12] Milletari, Fausto, et al., “V-Net: Fully Convolutional Neural Networks for Volumetric Medical Image Segmentation,” 2016 Fourth International Conference on 3D Vision (3DV), 565–571 (2016).
[13] Zhou, Dingfu, Song, et al., “IoU Loss for 2D/3D Object Detection,” 2019 International Conference on 3D Vision (3DV), 85–94 (2019).
[14] Oktay, O., et al., “Attention u-net: Learning where to look for the pancreas,” arXiv preprint arXiv:1804.03999, 2018.
[15] Badrinarayanan, V., et al., “Segnet: A deep convolutional encoder-decoder architecture for image segmentation,” IEEE transactions on pattern analysis and machine intelligence, 39(12), 2481-2495 (2017).
[16] Gu, Z., et al., “Ce-net: Context encoder network for 2d medical image segmentation,” IEEE transactions on medical imaging, 38(10), 2281-2292 (2019).
[17] Hu, Jie, et al., “Squeeze-and-excitation networks,” in Proceedings of the IEEE conference on computer vision and pattern recognition, 7132-7141 (2018).

Downloaded From: https://www.spiedigitallibrary.org/conference-proceedings-of-spie on 05 Apr 2022
Terms of Use: https://www.spiedigitallibrary.org/terms-of-use